Renew. Energy Environ. Sustain. **6**, 6 (2021)

https://doi.org/10.1051/rees/2021006

Renewable Energy and Environmental Sustainability

Available online at:
www.rees-journal.org

RESEARCH ARTICLE OPEN ACCESS

Economic assessment of WECS for water pumping systems in the North Region of Cameroon

Dieudonné Kaoga Kidmo[1,*], Bachirou Bogno[2,3], Kodji Deli[1], Michel Aillerie[3], Bello Pierre Ngoussandou[1]

[1] Department of Renewable Energy, National Advanced School of Engineering of Maroua, University of Maroua, P.O. Box 46 Maroua, Cameroon
[2] Department of Physics, Higher Teachers' Training College, University of Maroua, P.O. Box 46 Maroua, Cameroon
[3] Laboratoire Matériaux Optiques, Photonique et Systèmes, LMOPS, EA 4423, Université de Lorraine, Metz, 57070, France

Received: 20 December 2020 / Received in final form: 15 March 2021 / Accepted: 16 March 2021

Abstract. This paper analyses the potential utilization of wind electric pumping for water distribution in off-grid locations of the North Region of Cameroon (NRoC), using ground measured data as well as long-term satellite-derived data. Furthermore, this paper puts emphasis on statistical indexes of accuracy for the comparison of measured (2007–2012) and long-term satellite-derived (2005–2020) data. The outcome of this study clearly indicates that long-term satellite-derived data, obtained through the Prediction of Worldwide Renewable Energy Resources, can be considered as a viable alternative to missing site-specific data from ground stations, mainly in developing countries. The accuracy of satellite-based wind resource is deemed sufficient to provide a reasonable assessment in the initial phase of wind project planning, before in situ measurements with high accuracy are available. To model wind speeds characteristics, the energy pattern factor method (EPF) has been utilized as one of the reliable Weibull distribution methods for the assessment of wind energy potential at desired turbines heights in the selected locations. Five 20-kW pitch-controlled wind turbines (WT) with a hub height of 30 m, are considered to evaluate the power output and energy produced. Volumetric flow rates and costs of water produced are estimated. The results showed that, out of the eight chosen locations, Figuil shows the best combination of capacity factors (CF) and costs of energy (COE), while the site of Poli displays the worst values of CF and COE, no matter which of the five WT is employed. Thus, selecting WT for low wind speeds regimes, should require to combine location wind resource and WT characteristics such as lower cut-in wind speed (1.5 m/s) as well as lower rated wind speed (8.0 m/s) in order to successfully and affordably implement the wind technology in the NRoC.

1 Introduction

The sustainable development of a country is closely linked to the utilization of renewable energy resources (RES) at its disposal [1]. RES provide not only an important source of employment, wealth and profits to the country, but also play a critical role in building a sustainable and modern society [2–4]. Cameroon is endowed with conventional sources of energy such as natural gas and oil fuels, however associated with the emissions of both air pollutants, greenhouse gases and global warming. These conventional sources of energy share the fuel sources for electrical energy production (natural gas and oil fuels) in the country and other energy needs of industries and populace [5]. Moreover, fossil fuel sources, which are gradually depleting, need to be preserved and utilized efficiently [6]. As the global energy demand increases and fossil fuels become a gradually expensive commodity to humankind, the focus has been shifted towards renewable energy for a sustainable development [7].

RES, such as biomass, geothermal, hydro, solar, wind are inexhaustible, clean, free and offer many benefits such as non-polluting and almost inexhaustible characteristics in contrast to fossil fuel [8]. To further add to RES advantages, they can be harnessed on a local basis for applications, such as decentralized production of electricity in remote or rural areas, with low density of population [9].

* e-mail: kidmokaoga@gmail.com

Amongst RES, wind energy is one of the world's most abundant and permanent energy source, with a high-level of utilization. In addition, the potential of wind energy is credited, in the best of cases, with forty times the global electricity demand [10]. Over the last twenty years, the yearly growth rate of global wind energy has achieved an average growth rate of 22% [11]. Wind energy conversion systems (WECS) are considered as a mature and cost-competitive technology for electricity production [12], which is produced locally [13], but its dissemination remains marginal in most African countries. WECS necessitate to correctly characterize the wind resource over a location in addition to its geographic distribution [14]. As result, wind power is poised to play a key role in meeting global growing demand for electricity, especially in developing countries such as Cameroon, where it can be harnessed at an affordable cost on a local basis for water pumping applications.

The NRoC lays in a low wind speed regime and as a result the region is faced with numerous challenges in developing wind energy [15]. Measured wind data are mostly available at the ground measurements station at the Garoua main airport, while for the seven other considered sites located beyond a radius of at least 50 km of the main measuring wind station, there are no ground measurements stations. Therefore, long-term satellite-derived data [16], obtained through the POWER (Prediction of Worldwide Renewable Energy Resources), are deemed suitable and a viable alternative to missing site-specific data from ground stations [17–19]. These satellite-derived data are at daily level, at a 0.5×0.5-degree resolution. Additional scientific literature related to the use of long-term satellite-derived data and their accuracy in comparison with in situ measurements are provided as referenced [20–23].

The aim of this paper is to acknowledge the use of satellite-based wind resource as appropriate data to provide a reasonable assessment, before higher-accuracy in situ measurements are accessible. Furthermore, this work explores wind power production using electric systems for water pumping in the NRoC. Measured wind speeds at 10 m height above ground level (agl), in hourly time-series format, from January 2007 to January 2012 were collected through a cup-generator anemometer for Garoua. When measured ground level data remained non-existent, satellite-derived data for the sites of Bashéo, Beka, Figuil, Pitoa, Poli, Rey-Bouba and Touboro, were obtained from the NASA Langley Research Center (LaRC) POWER Project funded through the NASA Earth Science/Applied Science Program [24]. The accuracy of satellite-derived data for Garoua (the only site with ground measurements) was assessed using statistical indexes of accuracy, namely coefficient of determination (R^2), index of agreement (IOA), mean bias error (MBE), root mean square error (RMSE) and relative root mean square error (RRMSE).

Kidmo et al. [5] summarized most recent studies performed across Cameroon to investigate wind speeds and power characteristics, wind energy and costs of WECS. Recent and relevant research studies related to Garoua are detailed as followed. Kidmo et al. [25] performed a statistical analysis of wind speed distribution using six Weibull Methods for wind power assessment. Kidmo et al. [26] evaluated wind energy potential for small scale water pumping. Less attention was so far paid to the combination of location wind resource and wind turbines (WT) characteristics such as cut-in wind speed as well as rated wind speed. This paper highlights the use of low wind speeds WT to take full advantages of local wind resource and WT characteristics. Capacity factors (CF), costs of energy generated (XAF/kWh) and water produced (XAF/m^3) are estimated using the Present Value Cost (PVC) method of energy produced per year, considering the frequency at which WT produce power.

To model wind speeds characteristics, the energy pattern factor method (EPF) [27,28] has been utilized as one of the reliable Weibull distribution methods for the assessment of wind energy potential at desired turbines heights in the selected locations. Five 20-kW pitch-controlled WT with a hub height of 30 m, are considered to evaluate the power output and energy produced. Volumetric flow rates and costs of water produced are estimated using a 50 m pumping head, for the sake of simplicity. The results showed that, out of the eight chosen locations, Figuil shows the best combination of capacity factors (CF) and costs of energy (COE), while the site of Poli displays the worst values of CF and COE, no matter which of the five WT is employed. Thus, selecting WECS for low wind speeds regimes, should require to combine location wind resource and WT characteristics such as lower cut-in wind speed (1.5 m/s) as well as lower rated wind speed (8.0 m/s) in order to successfully and affordably implement the wind technology in the NRoC.

2 Methodology

2.1 Study area

The North Region as shown in Figure 1, is one of the ten regions of Cameroon, Located between 7.30 − 10.00 N latitude and 12.30 − 15.00 E longitude. It covers an area of 66 090 km^2 and is bordered by two regions of the country, the Far North Region to the north and the Adamawa Region to the south, Chad to the east, Central African Republic to the southeast and Nigeria to the west. The North region accounts for one of the driest regions of Cameroon under the influence of the harmattan winds in the dry season which lasts eight months, temperatures rise at their highest (40–45 °C) and there is no rainfall. During the rainy season which lasts four months, average rainfall is between 900 and 1500 mm and torrential rains are observed as well as lower temperatures compared to dry season. The Benoue depression constitutes the primary land feature of the North region, with an elevation in the range of zero to 200 m. Land elevations are in the range of 200–500 and 500–1000 m, respectively in the north and south of the region [29]. The selected sites, namely, Bashéo, Beka, Figuil, Garoua, Pitoa, Poli, Rey-Bouba and Touboro, as

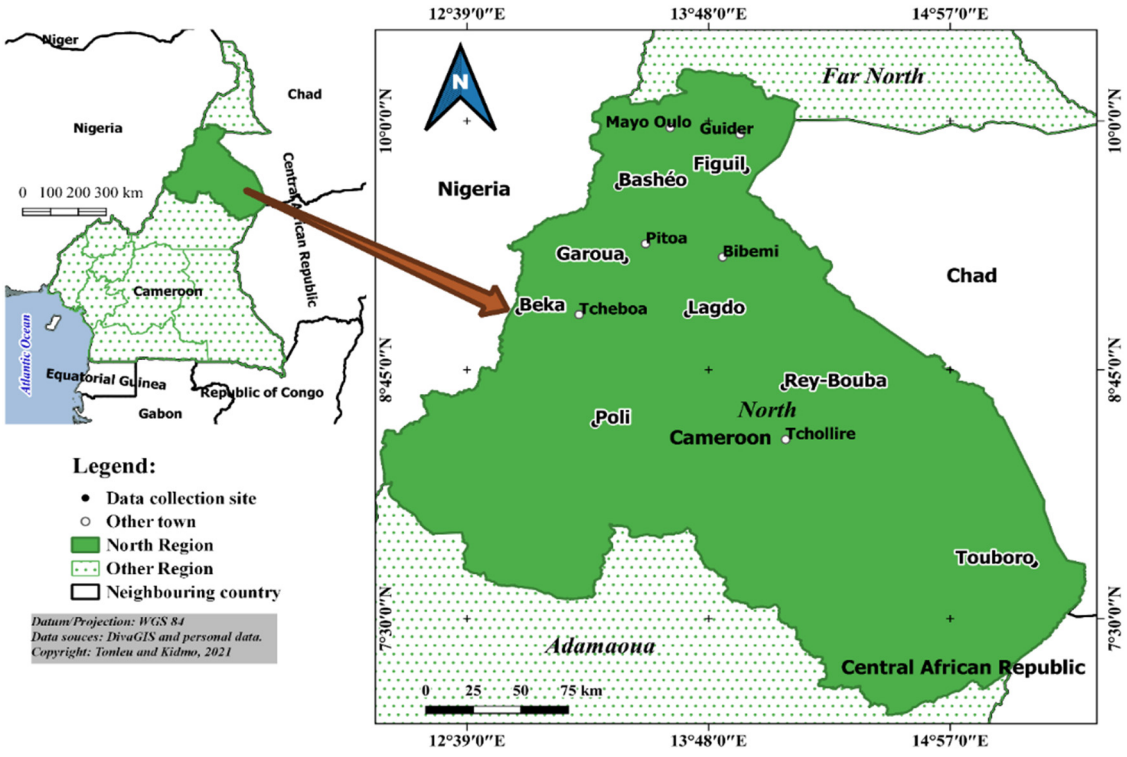

Fig. 1. Map showing the eight selected sites of the North Region of Cameroon.

shown in Figure 1, have been chosen based on relevant landscape information they provide in order to fully assess the potential of wind energy in the NRoC.

2.2 Wind data description and source

Two sources of data have been utilized in this work, measurements from a ground station for the site of Garoua and long-term satellite-derived data for the seven other sites. Wind speed measurements for the locality of Garoua, at 10 m height agl, in hourly time-series format, from January 2007 to January 2012 have been collected through a cup-generator anemometer at the Garoua, main meteorological station [25]. For the seven other selected sites of the north region, measured ground level data are non-existent. Therefore, long-term daily satellite-derived data, from January 2005 to January 2020, obtained through the POWER, have been utilized. These data were obtained from the NASA Langley Research Center (LaRC) POWER Project funded through the NASA Earth Science/Applied Science Program [24]. Table 1 provides geographical coordinates of the eight sites, as well as mean ambient temperature and measurement period.

2.3 Mean wind speed and standard deviation

Monthly mean wind speed v_m and standard deviation σ of wind speed data are calculated as Equations (1) and (2) [25]:

$$v_m = \frac{1}{N}\left(\sum_{i=1}^{N} v_i\right) \tag{1}$$

$$\sigma = \left[\frac{1}{N-1}\sum_{i=1}^{n}(v_i - v_m)^2\right]^{1/2} \tag{2}$$

Where:

v_m = mean wind speed [m/s]
σ = standard deviation of the mean wind speed [m/s]
v_i = wind speed [m/s]
N = number of wind speed data.

After the statistical analysis of wind data, monthly mean wind speeds and standard deviations for Garoua using measured and satellite-derived data, are summarized in Table 2, while Figures 2 and 3 show, respectively monthly mean wind speeds and standard deviations using satellite-derived data for for Bashéo, Beka, Figuil, Garoua, Pitoa, Poli, Rey-Bouba and Touboro. The magnitude of monthly mean measured wind speeds and standard deviations for Garoua at 10 m height agl, lay respectively within the range of 1.24 to 2.71 m/s and 0.73 to 1.39 m/s, while corresponding values using satellite-derived data range from 1.67 to 3.38 m/s and from 0.47 to 1.00 m/s, in that order.

2.4 Weibull probability density function

The Weibull probability density function (PDF), which is a special case of a generalized two-parameter Gamma distribution, has been extensively utilized in scientific literature for wind speed forecasting and wind energy potential assessment [30–32]. Weibull PDF can be characterized by its PDF $f(V)$ using Equation (3) and cumulative distribution function (CDF), $F(V)$ using

Table 1. Geographical data for eight selected sites of the North Region.

Location	Latitude (°)	Longitude (°)	Elevation (m)	Ambient temperature (°C)	Satellite Measurement period	In situ Measurement period
Bashéo	9.6721	13.3711	403.8	27.47	Jan 2005–Jan 2020	
Beka	9.0437	12.8982	296.16	27.90	Jan 2005–Jan 2020	
Figuil	9.7524	13.976	407.05	27.67	Jan 2005–Jan 2020	
Garoua	9.2955	13.3998	291.79	28.19	Jan 2005–Jan 2020	Jan 2007–Jan 2012
Lagdo	9.2862	13.3766	291.79	28.19	Jan 2005–Jan 2020	
Poli	8.4785	13.2595	512.62	26.67	Jan 2005–Jan 2020	
Rey-Bouba	8.6633	14.1595	344.08	28.17	Jan 2005–Jan 2020	
Touboro	7.7739	15.3489	651.63	25.96	Jan 2005–Jan 2020	

Table 2. Monthly mean wind speeds and standard deviations for Garoua using measured and satellite-derived data.

Period	**Measured**		**Satellite-derived**	
	v_{mG}	σ_G	v_{mS}	σ_S
Jan	1.585	0.920	3.21	0.84
Feb	1.588	0.930	3.38	0.95
Mar	2.093	1.057	3.35	1.00
Apr	2.711	1.385	3.09	0.92
May	2.511	1.256	2.54	0.69
Jun	2.492	1.296	2.31	0.74
Jul	2.333	1.287	2.22	0.66
Aug	1.840	1.017	2.04	0.63
Sep	1.603	0.884	1.67	0.47
Oct	1.583	0.949	1.70	0.49
Nov	1.395	0.870	2.21	0.64
Dec	1.237	0.733	2.88	0.70
Whole Year	1.915	1.168	2.55	0.68

Equation (4) [33]:

$$f(v) = \left(\frac{k}{C}\right).\left(\frac{v}{C}\right)^{k-1}.\exp\left[-\left(\frac{v}{C}\right)^{k}\right] \tag{3}$$

$$F(v) = 1 - \exp\left[-\left(\frac{v}{C}\right)^{k}\right] \tag{4}$$

Where:
$f(v)$ = probability of observing wind speed v;
v = wind speed [m/s];
C = Weibull scale parameter [m/s];
k = Weibull shape parameter.

Weibull parameters k and C are typically obtained using well-established estimation methods [25,34]. In this paper, Weibull parameters are computed using the energy pattern factor method (EPF). The first step is to define the power density expressed using Equation (5) [35].

$$P_d = \frac{1}{2}\rho\left(\frac{v}{C}\right)\int_0^{\infty} v^3 f(v)dv \tag{5}$$

Where:
ρ = air density at the site;

The air density (in kilograms per cubic meter) at a given location is calculated as the mass of a quantity of air (in kg) divided by its volume (in cubic meter). It depends on elevation and temperature above sea level and can be computed [36] using Equation (6).

$$\rho_a = \frac{353.049}{T} e^{\left(-0.034\frac{Z}{T}\right)} \tag{6}$$

Where:
Z = elevation (m);
T = temperature at the considered site (°K).

The second step of the EPF method is to determine the energy pattern factor (E_{pf}), as Equation (7) [37]:

$$E_{pf} = \frac{(v^3)_m}{(v_m)^3} = \frac{\left(\frac{1}{n}\sum_{i=1}^{n} {v_i}^3\right)}{\left(\frac{1}{n}\sum_{i=1}^{n} v_i\right)^3} \tag{7}$$

Where:
v_m = mean wind speed [m/s];
$(v^3)_m$ = mean of wind speed cubes.

Once the energy pattern factor is calculated by using Equation (7), the Weibull shape parameter is estimated from Equation (8) [38]:

$$k = 1 + \frac{3.69}{(E_{pf})^2} \tag{8}$$

where k is the dimensionless shape parameter illustrating how peaked the wind distribution is, while the scale parameter C indicates how 'windy' the wind location under consideration is [39].

The scale parameter is obtained using Equation (9):

$$C = \frac{v_m}{\Gamma\left(1 + \frac{1}{k}\right)} \tag{9}$$

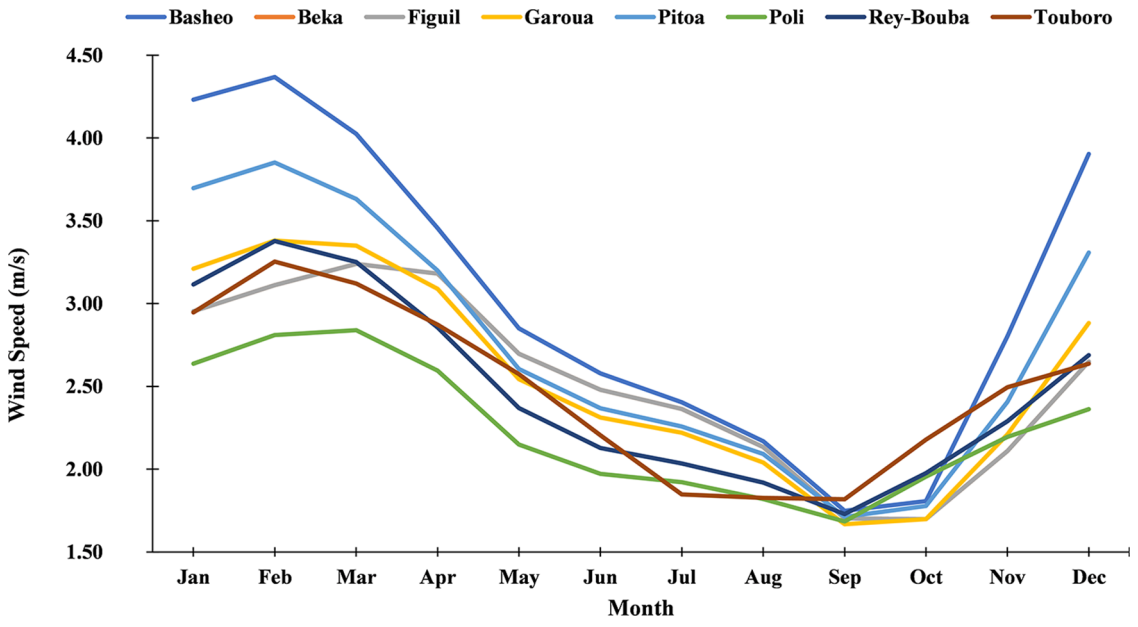

Fig. 2. Monthly mean wind speeds using satellite-derived data for Bashéo, Beka, Figuil, Garoua, Pitoa, Poli, Rey-Bouba and Touboro.

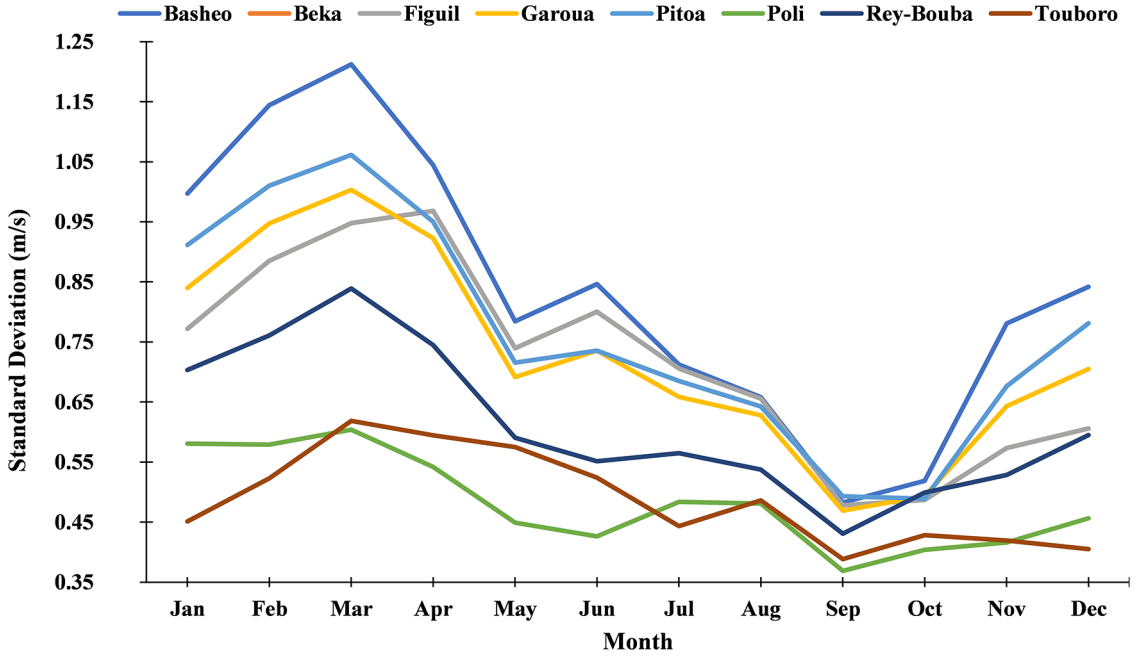

Fig. 3. Monthly standard deviations using satellite-derived data for Bashéo, Beka, Figuil, Garoua, Pitoa, Poli, Rey-Bouba and Touboro.

Where the standard gamma function is given by [40]:

$$\Gamma(x) = \int_0^\infty t^{x-1} \exp(-t) dt \tag{10}$$

The gamma function can be approximated by [25,41]:

$$\Gamma(x) = \left(\sqrt{2\pi x}\right)(x^{x-1})(e^{-x}) \times \left(1 + \frac{1}{12}x + \frac{1}{288}x^2 - \frac{139}{51840}x^3 + \ldots\right) \tag{11}$$

2.5 Statistical indexes of accuracy

In order to evaluate the performance of the considered satellite-derived data of Garoua, the following statistical indexes of accuracy are utilized:

1. Mean Bias Error (MBE) of satellite-derived values using Equation (12) [42,43]:

$$MBE = \left[\frac{1}{N}\sum_{i=1}^{N}(Sat_i - Gr_i)^2\right]^{1/2} \tag{12}$$

where Gr_i denotes cumulative frequency distribution (CFD) of measured values at wind speed v_i, in time step i, Sat_i the respective satellite-derived value, and N the number of non-zero wind speed data points. MBE provides basically the difference between CFD of average satellite-derived and average measured values. Satellite-derived values are overestimated if $MBE > 0$, while they are underestimated if $MBE < 0$.

2. Root mean square error (RMSE) using Equation (13) [44,45]:

$$RMSE = \left[\frac{1}{N}\sum_{i=1}^{N}(Sat_i - Gr_i)^2\right]^{1/2} \tag{13}$$

RMSE provides the deviation between satellite-derived and measured values. Successful forecasts correspond to low values of RMSE, while higher indicate deviations [43]. RMSE should be as close to zero as possible.

3. Relative root mean square error (RRMSE) using Equation (14) [30,46]:

$$RRMSE = \frac{\left[\frac{1}{N}\sum_{i=1}^{N}(Sat_i - Gr_i)^2\right]^{1/2}}{\frac{1}{N}\sum_{i=1}^{N}Gr_i} \times 100 \tag{14}$$

RRMSE is calculated by dividing RMSE to the average of CFD of measured values. Ratings of satellite-derived values' accuracy can be defined as [47]:

Excellent:	RRMSE < 10%;
Good:	10% < RRMSE < 20%;
Fair:	20% < RRMSE < 30%;
Poor:	RRMSE > 30%.

4. Coefficient of determination (R^2) using Equation (15) [30,48]:

$$R^2 = 1 - \frac{\sum_{i=1}^{N}(Gr_i - Sat_i)^2}{\sum_{i=1}^{N}(Gr_i - \overline{Sat_i})^2} \tag{15}$$

R^2 determines the linear relationship between CFD of average satellite-derived and average measured values. A higher R^2 represents a better fit using satellite-derived data and the highest value it can get is 1.

Where: Gr_i is the i^{th} CFD of ground (measured) wind speeds, Sat_i is the i^{th} CFD of satellite-derived wind speeds, $\overline{Sat_i}$ is the mean value of Sat_i, N the number of non-zero wind speed data points.

5. Index of Agreement (IOA) using Equation (16) [30,49]:

$$IOA = 1 - \frac{\overline{Sat_i} - \overline{Gr_i}}{\sum_{i=1}^{N}(|Sat_i - \overline{Gr_i}| + |Gr_i - \overline{Gr_i}|)^2} \tag{16}$$

Where: $\overline{Gr_i}$ denotes the average of Gr_i, $\overline{Sat_i}$ is the mean value of Sat_i, N the number of non-zero wind speed data points. IOA estimates the accuracy of satellite-derived wind speeds in predicting ground (measured) wind speeds. IOA values range from zero to one. IOA values above 0.5 imply efficiency in using satellite-derived data [43]

2.6 Extrapolation of wind speeds at different hub heights

In this study, five WT, using a 30 m hub height have been considered. Wind speeds data obtained at 10 m height agl, are therefore adjusted to the relevant WT hub height. The vertical extrapolation of scale and shape parameters at an elevation (z), is defined by the relationships in Equations (17) and (18) [50,51]:

$$C_z = C_{10} \times \left(\frac{z}{z_{10}}\right)^n \tag{17}$$

$$k_z = \frac{k_{10}}{1 - 0.00881\ln(z/10)} \tag{18}$$

Where z and z_{10} are in meters and the power law exponent n is given by Equation (19):

$$n = [0.37 - 0.088\ln(C_{10})] \tag{19}$$

Where, the scale C_{10} and shape k_{10} parameters are determined at 10 m height agl.

2.7 Mean wind power density and energy density

Wind power density ($P(v)$), in watts per square meter, is estimated using Equation (20) [52].

$$P(v) = \frac{1}{2}\rho A v^3 \tag{20}$$

The mean wind power density (p_D) based on the Weibull probability density function can be calculated using Equation (21) [33].

$$p_D = \frac{P(v)}{A} = \frac{1}{2}\rho C^3 \Gamma\left(1 + \frac{3}{k}\right) \tag{21}$$

The mean energy density (E_D) over a period of time T is expressed as Equation (22).

$$E_D = \frac{1}{2}\rho C^3 \Gamma\left(1 + \frac{3}{k}\right) T \tag{22}$$

Where:

ρ = air density at the site;
A = swept area of the rotor blades [m^2].

2.8 Wind turbine and electric pumping systems

Five WT, from different manufacturers are considered, as illustrated by Table 3. The five WT are represented by WT_1, WT_2, WT_3, WT_4, and WT_5 to avoid using registered names, trademarks etc. These WT are designed for low

Table 3. Characteristics of the selected wind turbines.

Characteristics	WT_1	WT_2	WT_3	WT_4	WT_5
Hub height (m)	30	30	30	30	30
Rated power $\boldsymbol{P_R}$ (kW)	20	20	20	20	20
Rotor diameter **(m)**	10	10	10	10	10
Cut-in wind speed $\boldsymbol{V_C}$ (m/s)	1.5	2.0	2.5	3.0	3.5
Rated wind speed $\boldsymbol{V_R}$ (m/s)	8	9	10	11	12
Cut-off wind speed $\boldsymbol{V_F}$ (m/s)	25	25	25	25	25
Price (USD/kW) [53]	1,775	1,775	1,775	1,775	1,775
Price (kXAF/kW)	1,065	1,065	1,065	1,065	1,065

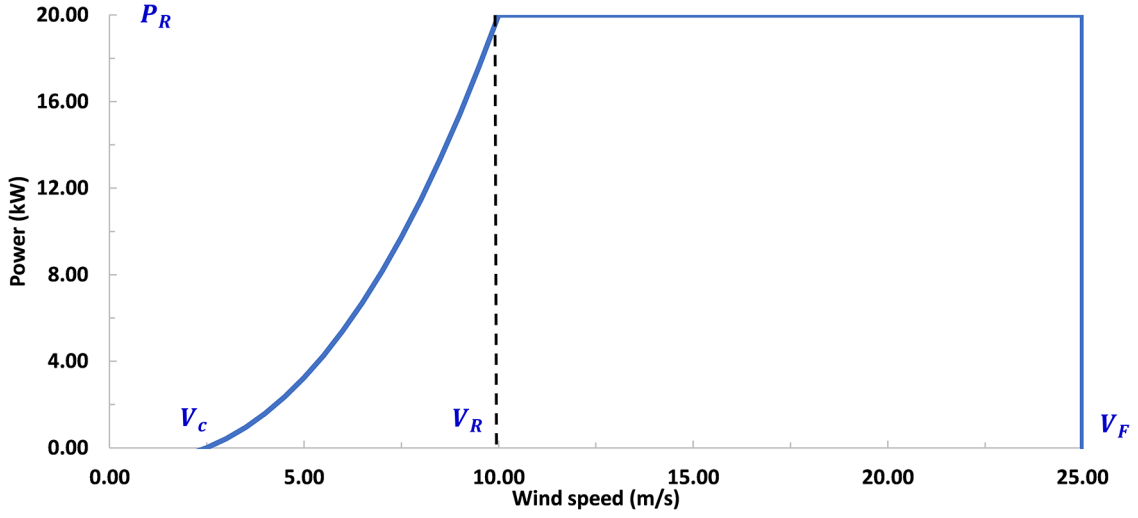

Fig. 4. Power Curve of a 20-kW pitch-controlled WT, with technical specifications of WT_3.

wind power density regime, for locations falling into Class 2 or lesser, based on PNL wind power classification scheme [50]. Although a 50 m pumping head is considered to calculate volumetric flow rates, a different pumping head can be considered, since the volumetric flow rate of water is inversely proportional to the pumping head.

2.9 Power curve model and capacity factor

The typical power curve of a 20-kW pitch-controlled WT is shown in Figure 4. Four different zones are observed as illustrated. For WS in the range of zero to cut-in wind speed (V_C), there is no output yielded. From the cut-in to rated WS (V_C to V_R), the power increases with the wind speed (WS). The power output curve is assumed to show a quadratic power shape, based on the selected power curve model in this work. From the rated WS (V_R) to the cut-out WS (V_F), the WT yields a constant output at the rated power (P_R), regardless of WS variations. For WS higher than V_F, there is no output yielded.

2.10 Power curve model and capacity factor

The power curve model of a WT can be modelled by four parameters: the cut-in wind speed (v_c), the rated wind speed (v_R), the cut-off wind speed (v_F) and the rated electrical power (P_{eR}). In this study, the power output curve model of a WT can be approximated with the parabolic law, using the combination of Equation (23) [54]:

$$P_e = \begin{cases} 0 & (v < v_c) \\ P_{eR}\dfrac{v^k - {v_c}^k}{{v_R}^k - {v_c}^k} & v_c \le v \le v_R \\ P_{eR} & v_R \le v \le v_F \\ 0 & (v_F < v) \end{cases} \quad (23)$$

The average power output ($P_{e,ave}$) from the turbine, which is related to the total energy production can be determined from Weibull distribution as Equation (24):

$$P_{e,ave} = P_{eR}\left\{\frac{e^{-\left(\frac{v_c}{C}\right)^k} - e^{-\left(\frac{v_R}{C}\right)^k}}{\left(\frac{v_R}{C}\right)^k - \left(\frac{v_c}{C}\right)^k} - e^{-\left(\frac{v_F}{C}\right)^k}\right\} \quad (24)$$

The capacity factor CF is defined as the ratio of the average power output ($P_{e,ave}$) to the rated electrical power (P_{eR}) of the WT. The capacity factor CF can thus be

computed as Equation (25) [55]:

$$CF = \left\{ \frac{e^{-\left(\frac{v_c}{C}\right)^k} - e^{-\left(\frac{v_R}{C}\right)^k}}{\left(\frac{v_R}{C}\right)^k - \left(\frac{v_c}{C}\right)^k} - e^{-\left(\frac{v_F}{C}\right)^k} \right\} \tag{25}$$

2.11 Water pumping capacity

The net hydraulic power output (P_{out}) required to deliver a volume of water $V_w(m^3)$ can be expressed using Equation (26) [56].

$$P_{out} = \frac{\rho_w \cdot g \cdot V_w \cdot H}{\eta T} = \frac{\rho_w \cdot g \cdot Q_w \cdot H}{\eta} \tag{26}$$

Where:

Q_w = volumetric flowrate $[m^3/day]$;
ρ_w = water density $[kg/m^3]$;
g = acceleration due to gravity $[m/s^2]$;
H = pump head [m]; η = system efficiency.

The volumetric flow rate of water is therefore evaluated using Equation (27).

$$\boldsymbol{Q_w} = \frac{\eta \cdot \boldsymbol{P}_{\text{out}}}{\rho_w \cdot \boldsymbol{g} \cdot \boldsymbol{H}} \tag{27}$$

When taking into account the efficiency of the pump ($\eta_{PUMP} = 62\%$ for the submersible electric pump model) the water pumping capacity rate (F_w) can be expressed as Equation (28).

$$F_w = 367 \times \eta_{PUMP} \cdot P_{out} \tag{28}$$

2.12 Costs analysis

In this work, the adopted method to evaluate the costs of energy (COE) and costs of water (COW) produced is the present value of costs (PVC) of energy produced per year using Equation (29) [57].

$$PVC = I + C_{om}\left(\frac{1+i}{r-i}\right) \times \left(1 - \left(\frac{1+i}{1+r}\right)^n\right) - S\left(\frac{1+i}{1+r}\right)^n \tag{29}$$

Where the following assumptions are made to estimate the cost of energy produced by the considered WT:

- $\boldsymbol{I}$ is the investment cost, which includes the WT price in addition to 20% for civil works and other connections;
- Average specific WT cost per kW is USD 1175, for WT rated power between 20 and 200 kW [53]
- $\boldsymbol{n}$ is the useful lifetime of WT in years (20 yrs); $\boldsymbol{i_o}$ is the nominal interest rate (16%);
- $\boldsymbol{S}$ is the scrap value (10% of the WT price); $\boldsymbol{i}$ is the inflation rate (3.6%);
- $\boldsymbol{C_{om}}$ is the operation and maintenance costs (7.5% of the investment cost).

The discount rate ($\boldsymbol{r}$) is determined using Equation (30) [58]:

$$\boldsymbol{r} = \frac{\boldsymbol{i_0} - \boldsymbol{i}}{1 + \boldsymbol{i}} \tag{30}$$

The Wind availability (A) is determined using Weibull CDF of wind speeds at which WT produce energy. The total energy output (E_{WT}) over the WT lifetime (in kilowatt-hour) is computed as Equation (31).

$$E_W = 8760 \times A \times n \times P_R \times C_f \tag{31}$$

The cost of energy (COE) per unit kWh using the PVC method can be estimated using Equation (32).

$$COE = \frac{PVC}{E_W} \tag{32}$$

The annual volume of water V_w (m^3/year) produced by the WT is determined from Equation (33).

$$V_w = \frac{\eta \cdot E_w}{n \cdot \rho_w \cdot g \cdot H} \tag{33}$$

The cost of water (COW) per unit m^3 using the PVC method can be estimated using Equation (34).

$$COW = \frac{PVC}{n \cdot V_w} \tag{34}$$

3 Results and discussion

3.1 Measured vs satellite data

Average monthly Weibull CDF values helped to perform the statistical comparison between measured and satellite-derived data. Table 4 shows statistical indicators for the accuracy of satellite-derived wind speed for the site of Garoua, which is the only site with measured ground level data. With the exception of May, June and July, satellite-derived values are slightly overestimated (MBE > 0) for the rest of the year. The yearly average MBE value of 0.021 indicates a slight overestimation of satellite-derived data. MBE values are in all cases close to zero, which demonstrate a match between locally measured and long-term satellite-derived data. RMSE values range between 0.142 in February and 0.002 in May. These values, close to zero, show successful forecasts. RRMSE values, from April to November, are less than 10%, denoting an excellent accuracy of satellite-derived data. RRMSE values for January, February, March and December are good, with values ranging from 11.4% to 15.5%. Overall, the accuracy of satellite-derived data for yearly average is excellent, with a RRMSE value of 6.1%. R^2 values vary from 0.847 in May to 0.696 in December. R^2 value of the yearly average is 0.809. R^2 values are generally higher and represents a better fit using satellite-derived data. IOA values range between 0.993 and 1.000 and this implies efficiency in using satellite-derived data. Therefore,

Table 4. Statistical indicators for the accuracy of satellite-derived wind speed for Garoua.

Period	MBE	RMSE	RRMSE	R^2	IOA
Jan	0.053	0.133	14.6%	0.759	0.993
Feb	0.058	0.142	15.5%	0.757	0.993
Mar	0.043	0.103	11.4%	0.805	0.995
Apr	0.012	0.029	3.2%	0.841	0.999
May	−0.001	0.002	0.2%	0.847	1.000
Jun	−0.003	0.009	1.0%	0.848	1.000
Jul	−0.001	0.004	0.4%	0.843	1.000
Aug	0.007	0.021	2.3%	0.813	0.999
Sep	0.003	0.008	0.9%	0.792	1.000
Oct	0.004	0.011	1.2%	0.789	1.000
Nov	0.026	0.077	8.3%	0.745	0.996
Dec	0.051	0.139	15.0%	0.696	0.993
Yearly average	0.021	0.056	6.1%	0.809	0.998

Table 5. Annual wind characteristics at WT's hub height for the eight sites.

Location	k(−)	C(m/s)	V_m(m/s)	ρ(kg/m^3)	W_{PD}(W/m^2)	E_{PD}(kWh/m^2/day)
Bashéo	2.43	4.55	4.04	1.12	59.35	1.42
Beka	2.76	3.85	3.43	1.13	33.65	0.81
Figuil	2.37	4.73	4.19	1.12	67.52	1.62
Garoua	2.63	3.89	3.46	1.13	35.55	0.85
Pitoa	2.54	4.16	3.69	1.13	44.30	1.06
Poli	3.27	3.44	3.08	1.11	21.83	0.52
Rey-Bouba	2.89	3.78	3.37	1.12	30.88	0.74
Touboro	3.32	3.76	3.38	1.09	28.04	0.67

satellite-derived data can accurately represent measured data and when measured ground level data are missing, satellite-derived data can be suitable to assess the potential of wind energy. Similar studies on the use of satellite-derived data are found in the literature. Schmidt et al. [23] performed a comparison between in situ measurements of wind speed from Wave Glider (WG) and satellite/reanalysis products, including the wind speed error per wind speed category, RMSE, bias, and correlation coefficients. Accuracy values are within the same ranges as the present work. Barthelmie and Pryor [21] worked on satellite sampling of offshore wind speeds to represent wind speed distributions. Their study have stressed the difficulties to obtain through in situ methods wind speeds over the oceans. Remmers et al. [22] observed a very strong positive linear relationship between satellite-derived wind speed data and the in situ measurements. Ayompe and Duffy [59] assessed the energy generation potential of photovoltaic systems in Cameroon using satellite-derived solar radiation datasets due to the lack of a reliable network of surface observation stations for collecting weather data in the country. These studies concluded that the accuracy of satellite-derived data varies according to empirical model functions utilized. Besides, the accuracy of satellite-based wind resource is sufficient to provide a reasonable assessment in the initial phase of wind project planning, before higher-accuracy in situ measurements are available.

3.2 Wind characteristics

It is observed that the probability of observing higher wind speeds is highest for Figuil. In addition, the probability of observing lower wind speeds is highest for Poli. For each site, the average air density is based on daily average temperature and location values of elevation. Air density values in the North Region vary between 1.10 and 1.13 kg/m^3, while the corresponding elevations are in the range of 291.79–651.63 m. At 10 m height agl, annual average wind speeds range from 2.24 m/s for Poli to 3.16 m/s for Figuil, corresponding wind power densities vary from 8.43 W/m^2 for Poli to 28.89 W/m^2 for Figuil. With annual average wind power densities less than 100 W/m^2, the wind resource in the North Region can be ranked as wind power class 1, based on the scheme proposed by Battelle—Pacific Northwest Laboratory (PNL) [60]. Class 1 areas are considered unsuitable for large scale wind power development. It can be further observed that, for each of the eight sites, the peak of the PDFs, which indicates the most frequent wind speed, skews towards the higher values of wind speed. Table 5 proposes statistical Weibull analysis of

Table 6. Annual average frequency for wind speeds greater or equal to WT cut-in wind speed for different sites.

Location	WT_1	WT_2	WT_3	WT_4	WT_5
Bashéo	87.33%	76.15%	62.59%	48.21%	34.61%
Beka	84.20%	68.36%	49.46%	31.21%	16.83%
Figuil	87.95%	77.56%	64.95%	51.41%	38.32%
Garoua	83.44%	67.96%	49.90%	32.52%	18.53%
Pitoa	85.25%	71.80%	55.76%	39.53%	25.34%
Poli	82.91%	61.88%	36.97%	16.44%	5.04%
Rey-Bouba	84.48%	67.92%	47.87%	28.74%	14.29%
Touboro	87.69%	71.09%	48.90%	26.97%	11.24%

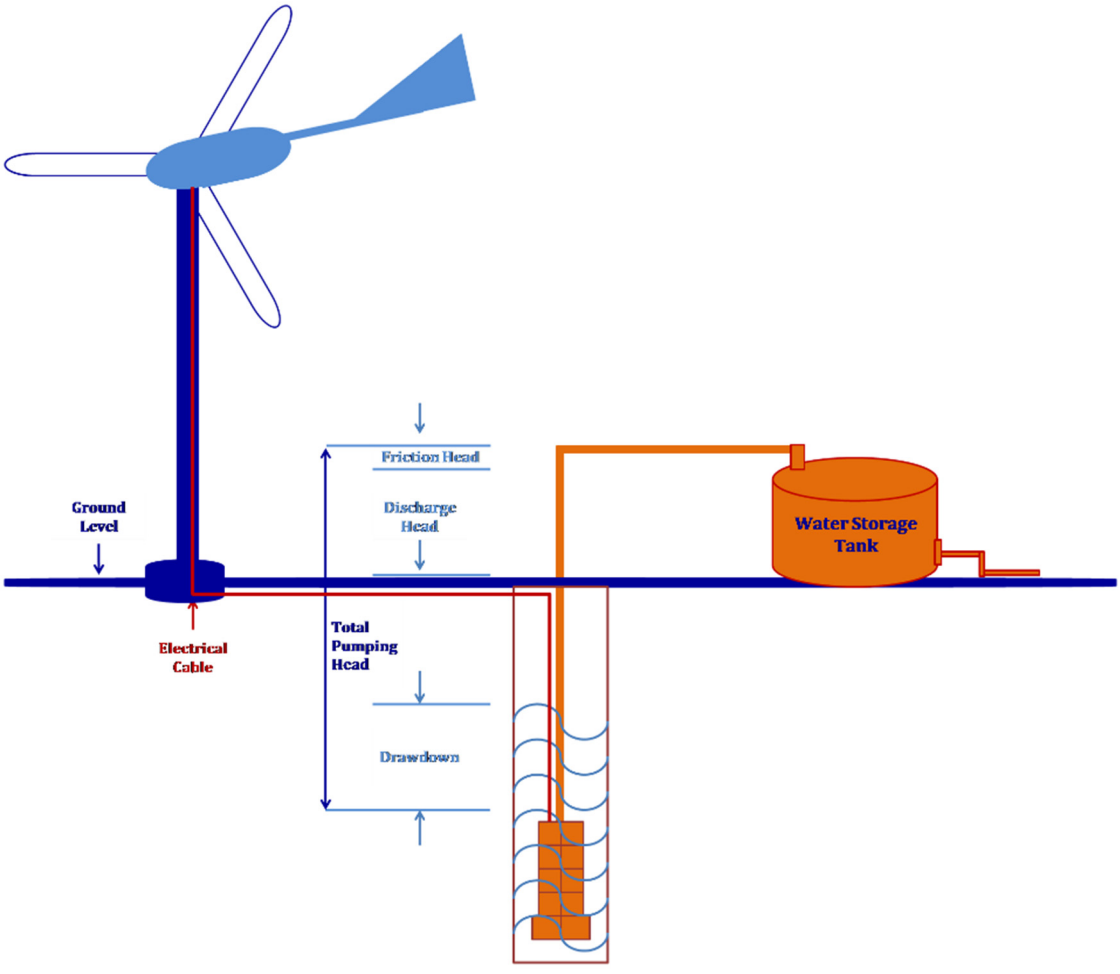

Fig. 5. Typical wind electric pumping systems (WEPS).

wind speed data for 30 m elevation (tower of WT) for the eight sites. For each site, the average air density was adjusted to reflect the 30 m-hub height tower. Annual average Weibull parameters were extrapolated to the 30 m height agl, as well as average wind speeds, power densities and energy densities.

Table 6 presents for WT_1, WT_2, WT_3, WT_4 and WT_5, the annual average frequency for wind speeds greater or equal to WT's cut-in wind speed for each of the eight selectd sites. It's observed that the probability of WT to produce power is the highest using WT_1, while this availability is the lowest using WT_5.

3.3 Wind turbine and WEPS

Figure 5 shows a typical wind electric pumping system. In order to highlight WECS characteristics needed for low wind speed locations, the five WT, with a rated capacity of

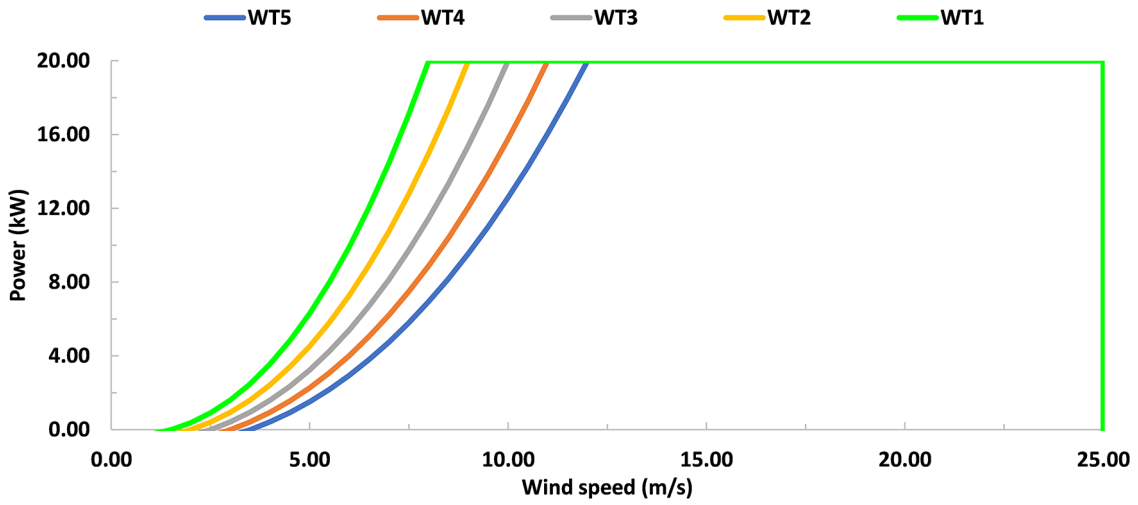

Fig. 6. Power curves of the five selected 20-kW pitch-controlled WT, which combine Figuil wind characteristics.

Table 7. CF and COE using WT_1, WT_2, WT_3, WT_4, and WT_5, for the eight sites.

Location	WT_1		WT_2		WT_3		WT_4		WT_5	
	Cf	COE	Cf	COE	Cf	COE	Cf	COE	Cf	COE
Bashéo	23.70%	55.28	17.03%	88.20	12.12%	150.75	8.53%	278.22	5.90%	559.93
Beka	12.49%	108.77	8.31%	201.50	5.44%	425.52	3.45%	1062.82	2.09%	3248.33
Figuil	26.52%	49.05	19.41%	76.01	14.05%	125.39	10.06%	221.23	7.11%	420.17
Garoua	13.98%	98.07	9.43%	178.53	6.27%	365.88	4.05%	868.50	2.52%	2450.37
Pitoa	17.77%	75.51	12.31%	129.48	8.44%	243.20	5.68%	509.78	3.72%	1213.99
Poli	5.96%	231.43	3.67%	503.71	2.18%	1422.70	1.20%	5799.08	0.60%	38 066.24
Rey-Bouba	10.80%	125.33	7.07%	238.32	4.54%	526.41	2.81%	1416.48	1.65%	4856.66
Touboro	7.84%	166.42	4.93%	326.28	3.05%	767.44	1.80%	2356.00	0.99%	10 301.13

20 kW and a 30 m tower hub height, were considered for uniformity in the comparison. These WT are represented by WT_1, WT_2, WT_3, WT_4 and WT_5, to avoid the use of trade names. Cut-in and rated wind speeds are different for each of the five WT. WT_1 has the lowest cut-in and rated wind speeds, while WT_5 has the highest cut-in and rated wind speeds as illustrated by Table 3. Five 20-kW pitch-controlled WT, whose power curves are illustrated by Figure 6, combine Figuil wind characteristics with WT characteristics. The WECS are equipped with a submersible electric pump model to produce energy from wind and pump water using the produced energy for each of the eight selected sites. For the purpose of this work, a total dynamic head of 50 m was adopted as the average in the NRoC. Any other pumping head could be used since the volumetric flow rate of water is inversely proportional to pumping head.

3.4 Cost of energy

Table 7 provides the values of capacity factors (CF) and costs of energy (COE), using WT_1, WT_2, WT_3, WT_4 and WT_5, for the eight chosen sites. The site of Figuil shows the best combination of CF and cost of energy, no matter the WT used, followed by the sites of Bashéo and Pitoa. The site of Poli displays the worst CF and COE. For the site of Figuil, the CF is equal to 26.52% and the COE is 49.05 XAF/kWh using WT_1. WT_5 shows the worst performance, with CF equal to 7.11% and COE equal to 420.17 XAF/kWh. WT_5 displays the poorest performance amongst WT.

3.5 Flow rate capacity

Figure 7 presents annual average flow capacity (m^4/h) for WT_1, WT_2, WT_3, WT_4 and WT_5 for the eight selected sites. Figuil shows the best flow rates capacity, 1076, 695, 421, 239 and 125.6 m^4/h, respectively using WT_1, WT_2, WT_3, WT_4 and WT_5. Poli displays the worst flow rates capacity, 228, 105, 37, 9 and 1.4 m^4/h. For the site of Figuil, the annual average flow capacity are 613.76, 412.67, 233.55 and 191.28 m^4/h, using WT_1, WT_2, WT_3, WT_4 and WT_5, in that order. WT_5 displays the poorest performance amongst WT.

3.6 Cost of water

Table 8 displays the costs of water (COW) and flow rate (m^3/day), using WT_1, WT_2, WT_3, WT_4 and WT_5, for the selected sites. It is observed that Figuil presents the best

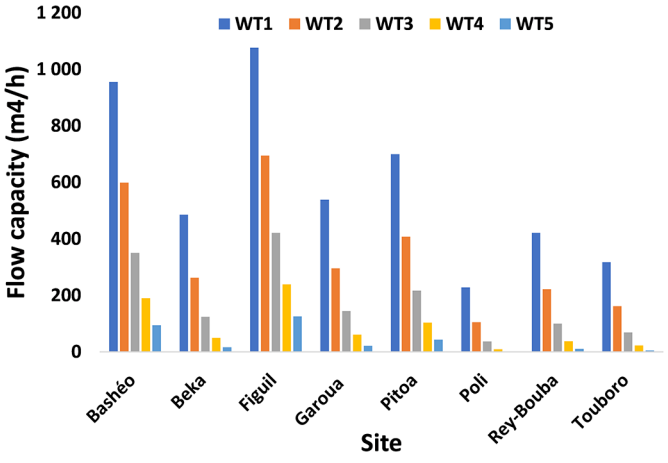

Fig. 7. Annual average flow capacity (m^4/h) for WT_1, WT_2, WT_3, WT_4 and WT_5 for the selected sites of the North Region.

combination of COW and flow rate energy, while Poli shows the worst values, independently of WT used. For a total dynamic head of 50 m, the COW for Figuil are 4.01, 9.63, 26.20, 81.57 and 294.23 XAF/m^3, respectively using WT_1, WT_2, WT_3, WT_4 and WT_5, while corresponding values of flow rate energy are 1515, 631, 232, 74 and 21 m^3/day. WT_5, in all cases, shows the poorest performance.

4 Conclusion

The economic assessment of wind energy conversions systems, for electric water pumping systems in the NRoC, has been explored, using measured and satellite-derived wind data. The accuracy of satellite-derived wind speeds data was assessed using MBE, RMSE, RRMSE, R^2 and IOA indicators. Satellite-based wind resources provided a reasonable accuracy and were deemed a viable alternative to missing site-specific data from ground stations in Bashéo, Beka, Figuil, Pitoa, Poli, Rey-Bouba and Touboro. The energy pattern factor method (EPF) modeled wind speeds characteristics for the assessment of wind energy potential at desired turbines heights in the selected locations. Five 20-kW pitch-controlled WT of 30 m hub height, assessed the power output and energy produced. The assessment of the wind resource at 10 m height agl showed average annual power densities in the range of 8.43–28.89 W/m^2. At 10 m height agl, this wind potential suggests that the NRoC falls under class 1 using the scheme proposed by Battelle-Pacific Northwest Laboratory (PNL). Therefore, the wind resource is deemed unsuitable for large scale WT applications. Hence, the need to use low wind speed WT such as WT_1 for electric water pumping applications. Based on its higher performance in comparison to the four other WT, WT_1, with the lowest cut-in (1.5 m/s) and rated (8.0 m/s) wind speeds, showed the highest capacity factors, thus the lowest costs of energy and water produced. As a result, cut-in and rated wind speeds have strong impact on the capacity factor, while cut-out wind speed has negligible impact on it. Choosing WT for low wind speeds regime, require to combine

Table 8. COW and volumetric flow rate using WT_1, WT_2, WT_3, WT_4, and WT_5, for the eight sites.

Location	WT_1		WT_2		WT_3		WT_4		WT_5	
	Vf (m^3/day)	COW (XAF/m^3)	Vf (m^3/day)	COW (XAF/m^3)	Vf (m^3/day)	COW (XAF/m^3)	Vf (m^3/day)	COW (XAF/m^3)	Vf (m^3/day)	COW (XAF/m^3)
Bashéo	1192.50	5.09	468.44	12.97	160.37	37.87	47.08	129.01	11.62	522.52
Beka	308.04	19.72	89.76	67.67	20.13	301.78	3.23	882.63	0.35	17 585.89
Figuil	1515	4.01	631	9.63	232	26.20	74	81.57	21	294.23
Garoua	379	16.03	114	53.12	27	223.11	5	1257.14	1	10 007.08
Pitoa	639	9.50	217	27.94	62	98.58	14	433.12	2	2456.28
Poli	68	89.26	14	422.87	2	3373.41	0	56 048.41	0	2 415 041.39
Rey-Bouba	232	19.07	64	61.25	13	246.35	2	1378.51	0	11 922.91
Touboro	132	46.16	34	177.43	6	981.60	1	9251.12	0	176 853.92

location wind resource and WT characteristics such as cut-in and rated wind speeds in order to successfully and affordably implement the wind technology in the NRoC.

Nomenclature

v_m	Mean wind speed [m/s]
k_{10}	Shape parameter at 10 m height agl [−]
k_z	Shape parameter at **z** meters height agl [−]
σ	Standard deviation of the mean wind speed [m/s]
n	Useful lifetime of WT in years (20 yrs) [year]
F_w	Water pumping capacity rate [m^4/h]
v_{mG}	Measured wind speed [m/s]
σ_G	Standard deviation of the mean measured WS [m/s]
v_{mS}	Satellite-derived wind speed [m/s]
σ_S	Standard deviation of the mean satellite-derived WS [m/s]
$f(v)$	Probability of observing wind speed v
g	Acceleration due to gravity [m/s^2]
C	Weibull scale parameter [m/s]
k	Weibull shape parameter [−]
E_{pf}	Energy pattern factor [−]
MBE	Mean Bias Error [−]
$RRMSE$	Relative root mean square error [%]
R^2	Coefficient of determination [−]
Gr_i	i^{th} CFD of ground (measured) wind speeds
Sat_i	i^{th} CFD of satellite-derived wind speeds
C_{om}	Operation and maintenance costs [%]
N	Number of non-zero wind speed data points
C_{10}	Scale parameter at 10 m height agl [m/s]
C_z	Scale parameter at **z** meters height agl [m/s]
E_{WT}	Total energy output over the WT lifetime [kWh]
V_w	Annual volume of water [m^3/year]
v_i	Wind speed [m/s]
N	Number of wind speed data
v	Wind speed [m/s]
n	Power law exponent [−]
v_c	Cut-in wind speed [m/s]
v_R	Rated wind speed [m/s]
v_F	Cut-off wind speed [m/s]
P_{eR}	Rated electrical power [kW]
$P_{e,ave}$	Average power output [kW]
Q_w	Volumetric flow rate (m^3/day)
ρ_w	Water density [kg/m^3]
$\overline{Sat_i}$	Mean value of Sat_i
H	Pump head [m]
η	System efficiency [−]
PVC	Present value of costs [XAF]
η_{PUMP}	Efficiency of the pump [−]
P_{out}	Net hydraulic power output [kW]
I	Investment cost [XAF]
i_o	Nominal interest rate [%]
S	Scrap value [%]
I	Inflation rate [%]
r	Discount rate [%]
COE	Cost of energy [XAF/kWh]
COW	Cost of water [XAF/m^3]
IOA	Index of Agreement
$RMSE$	Root mean square error [−]

The authors gratefully acknowledge the NASA Langley Research Center (LaRC) POWER Project funded through the NASA Earth Science/Applied Science Program for providing wind and temperature data used in this project.

References

1. K.O. Odeku, An analysis of renewable energy policy and law promoting socio-economic and sustainable development in rural South Africa, J. Hum. Ecol. **40**, 53–62 (2012)
2. U. Lehr, A. Mönnig, R. Missaoui, S. Marrouki, G. Ben Salem, Employment from renewable energy and energy efficiency in Tunisia – new insights, new results, Energy Procedia **93**, 223–228 (2016)
3. M.S. Salehudin, D.K. Prasad, P. Osmond, Renewable energy potential for energy efficient resort development in Malaysia, *Solar 2011, the 49th AuSES Annual Conference*, 2011, no. December, pp. 1–10
4. M.O. Oseni, An analysis of the power sector performance in Nigeria, Renew. Sustain. Energy Rev. **15**, 4765–4774 (2011)
5. D.K. Kidmo, K. Deli, B. Bogno, Status of renewable energy in Cameroon, Renew. Energy Environ. Sustain. **6**, 1–11 (2021)
6. O.S. Ohunakin, Assessment of wind energy resources for electricity generation using WECS in North-Central region, Nigeria, Renew. Sustain. Energy Rev. **15**, 1968–1976 (2011)
7. P.K. Halder, N. Paul, M.U.H. Joardder, M. Sarker, Energy scarcity and potential of renewable energy in Bangladesh, Renew. Sustain. Energy Rev. **51**, 1636–1649 (2015)
8. K.S. Elie Bertrand, K. Abraham, M. Lucien, Sustainable energy through wind speed and power density analysis in Ambam, South Region of Cameroon, Front. Energy Res. **8**, 1–9 (2020)
9. A. Fashina, M. Mundu, O. Akiyode, L. Abdullah, D. Sanni, L. Ounyesiga, The drivers and barriers of renewable energy applications and development in Uganda: a review, Clean Technol. **1**, 9–39 (2018)
10. D.A. Salam, A. Riadh, Wind energy state of the art: present and future technology advancements, Renew. Energy Environ. Sustain. **5**, 1–8 (2020)
11. D.K. Kidmo, B. Bogno, K. Deli, D. Goron, Seasonal wind characteristics and prospects of wind energy conversion systems for water production in the far North Region of Cameroon, Smart Grid Renew. Energy **11**, 127–164 (2020)
12. IRENA, Global renewables outlook: energy transformation 2050 (Abu Dhabi, 2020). www.irena.org/publications
13. M. Harries, Disseminating wind pumps in rural Kenya – meeting rural water needs using locally manufactured wind pumps, Energy Policy **30**, 1087–1094 (2002)
14. C. Fant, B. Gunturu, A. Schlosser, Characterizing wind power resource reliability in southern Africa, Appl. Energy **161**, 565–573 (2016)
15. J. Kenfack, J. Voufo, P.S. Ngohe Ekam, J.K. Lewetchou, U. Nzotcha, Overcoming local constraints when developing renewable energy systems for the electrification of remote areas in Africa, Renew. Energy Environ. Sustain. **5**, 1–10 (2020)

16. NASA, POWER Single Point Data Access (2021). https://power.larc.nasa.gov/data-access-viewer/ (accessed March 14, 2021)
17. J.W. White, G. Hoogenboom, P.W. Wilkens, P.W. Stackhouse Jr., J.M. Hoel, Evaluation of satellite-based, modeled-derived daily solar radiation data for the continental United States, Cimatol. Water Manag. **103**, 1242–1251 (2011)
18. J. Bai, X. Chen, A. Dobermann, H. Yang, K.G. Cassman, F. Zhang, Evaluation of nasa satellite-and model-derived weather data for simulation of maize yield potential in China, Agron. J. **102**, 9–16 (2010)
19. J.W. White, G. Hoogenboom, P.W. Stackhouse, J.M. Hoell, Evaluation of NASA satellite- and assimilation model-derived long-term daily temperature data over the continental US, Agric. For. Meteorol. **148**, 1574–1584 (2008)
20. C.B. Hasager et al., Remote sensing of environment offshore wind climatology based on synergetic use of Envisat ASAR, ASCAT and QuikSCAT, Remote Sens. Environ. **156**, 247–263 (2015)
21. R.J. Barthelmie, S.C. Pryor, Can satellite sampling of offshore wind speeds realistically represent wind speed distributions? J. Appl. Meteorol. **42**, 83–94 (2003)
22. T. Remmers, F. Cawkwell, C. Desmond, J. Murphy, E. Politi, The potential of advanced scatterometer (ASCAT) 12.5 km coastal observations for offshore wind farm site selection in Irish waters, 1–16 (2019)
23. K.M. Schmidt, S. Swaart, C. Reason, S.-A. Nicholson, Evaluation of satellite and reanalysis wind products with in situ wave glider wind observations in the Southern Ocean, J. Atmos. Ocean. Technol. **34**, 2551–2568 (2017)
24. NASA, NASA Surface meteorology and Solar Energy: RETScreen Data (2020). https://eosweb.larc.nasa.gov/cgi-bin/sse/sse (accessed Dec. 07, 2020)
25. D.K. Kidmo, R. Danwe, Y.S. Doka, N. Djongyang, Statistical analysis of wind speed distribution based on six Weibull Methods for wind power evaluation in Garoua, Cameroon, J. Renew. Energies **18**, 105–125 (2015)
26. D.K. Kidmo, N. Djongyang, S.Y. Doka, D. Raidandi, Assessment of wind energy potential for small scale water pumping systems in the north region of Cameroon, Int. J. Basic Appl. Sci. **3**, 38–46 (2014)
27. S.a. Akdağ, A. Dinler, A new method to estimate Weibull parameters for wind energy applications, Energy Convers. Manag. **50**, 1761–1766 (2009)
28. N. Izadyar, H. Chyuan, W.T. Chong, K.Y. Leong, Resource assessment of the renewable energy potential for a remote area: a review, Renew. Sustain. Energy Rev. **62**, 908–923 (2016)
29. North Region (Cameroon), From Wikipedia, Free Encycl., 2020. https://en.wikipedia.org/wiki/North%7B_%7DRegion%7B_%7D(Cameroon)%7B#%7DClimate (accessed Oct. 10, 2020)
30. K. Mohammadi et al., Assessing different parameters estimation methods of Weibull distribution to compute wind power density, Energy Convers. Manag. **108**, 322–335 (2016)
31. K. Mohammadi, O. Alavi, A. Mostafaeipour, N. Goudarzi, M. Jalilvand, Assessing different parameters estimation methods of Weibull distribution to compute wind power density, Energy Convers. Manag. **108**, 322–335 (2016)
32. P.A. Costa Rocha, R.C. de Sousa, C.F. de Andrade, M.E.V. da Silva, Comparison of seven numerical methods for determining Weibull parameters for wind energy generation in the northeast region of Brazil, Appl. Energy **89**, 395–400 (2012)
33. B. Safari, J. Gasore, A statistical investigation of wind characteristics and wind energy potential based on the Weibull and Rayleigh models in Rwanda, Renew. Energy **35**, 2874–2880 (2010)
34. P.A. Costa Rocha, R.C. de Sousa, C.F. de Andrade, M.E.V. da Silva, Comparison of seven numerical methods for determining Weibull parameters for wind energy generation in the northeast region of Brazil, Appl. Energy **89**, 395–400 (2012)
35. S.F. Khahro, K. Tabbassum, A.M. Soomro, L. Dong, X. Liao, Evaluation of wind power production prospective and Weibull parameter estimation methods for Babaurband, Sindh Pakistan, Energy Convers. Manag. **78**, 956–967 (2014)
36. B. Bailey, S. McDonald, D. Bernadett, M. Markus, K. Elsholz, Wind resource assessment handbook: fundamentals for conducting a successful monitoring program, Music Educ. J. **41**, 65 (1997)
37. A. Azad, M. Rasul, T. Yusaf, Statistical diagnosis of the best Weibull methods for wind power assessment for agricultural applications, Energies **7**, 3056–3085 (2014)
38. L. Bilir, M. İmir, Y. Devrim, A. Albostan, Seasonal and yearly wind speed distribution and wind power density analysis based on Weibull distribution function Science Direct Seasonal and yearly wind speed distribution and distribution function, Int. J. Hydrogen Energy **40**, 15301–15310 (2016)
39. I. Fyrippis, P.J. Axaopoulos, G. Panayiotou, Wind energy potential assessment in Naxos Island, Greece, Appl. Energy **87**, 577–586 (2010)
40. L. Olatomiwa, S. Mekhilef, O.S. Ohunakin, Hybrid renewable power supply for rural health clinics (RHC) in six geo-political zones of Nigeria, Sustain. Energy Technol. Assess. **13**, 1–12 (2016)
41. J.F. Manwell, J.G. McGowan, A.L. Rogers, Wind energy explained, Theory, Design and Application (BAffins Lane, Chichester, 2002)
42. A. De Meij et al., Wind energy resource mapping of Palestine, Renew. Sustain. Energy Rev. **56**, 551–562 (2016)
43. C. Stathopoulos, A. Kaperoni, G. Galanis, G. Kallos, Wind power prediction based on numerical and statistical models, J. Wind Eng. Ind. Aerodyn. **112**, 25–38 (2013)
44. T.P. Chang, Wind speed and power density analyses based on mixture Weibull and maximum entropy distributions, Int. J. Appl. Sci. Eng. **8**, 39–46 (2010)
45. D.K. Kidmo, R. Danwe, N. Djongyang, S.Y. Doka, Comparison of five numerical methods for estimating Weibull parameters for wind energy applications in the district of Kousseri, Cameroon, Asian J. Nat. Appl. Sci. **3**, 72–87 (2014)
46. C. Neme, Statistical analysis of wind speed profile: a case study from Iasi Region, Romania, Int. J. Energy Eng. **3**, 261–268 (2013)
47. K. Mohammadi, A. Mostafaeipour, O. Alavi, N. Goudarzi, M. Jalilvand, Assessing different parameters estimation methods of Weibull distribution to compute wind power density, Energy Convers. Manag. **108**, 322–335 (2016)
48. T.R.R. Ayodele, A.A.a. Jimoh, J.L.L. Munda, J.T.T. Agee, Wind distribution and capacity factor estimation for wind turbines in the coastal region of South Africa, Energy Convers. Manag. **64**, 614–625 (2012)
49. G. Gualtieri, S. Secci, Methods to extrapolate wind resource to the turbine hub height based on power law: a 1-h wind speed vs. Weibull distribution extrapolation comparison, Renew. Energy **43**, 183–200 (2012)

50. A. Mostafaeipour, M. Jadidi, K. Mohammadi, A. Sedaghat, An analysis of wind energy potential and economic evaluation in Zahedan, Iran, Renew. Sustain. Energy Rev. **30**, 641–650 (2014)
51. O.S.S. Ohunakin, M.S.S. Adaramola, O.M.M. Oyewola, Wind energy evaluation for electricity generation using WECS in seven selected locations in Nigeria, Appl. Energy **88**, 3197–3206 (2011)
52. A.N. Celik, A. Albani, M.Z. Ibrahim, A statistical analysis of wind power density based on the Weibull and Rayleigh models at the southern region of Turkey, Renew. Energy **29**, 593–604 (2004)
53. S. Diaf, G. Notton, D. Diaf, Technical and economic assessment of wind farm power generation at Adrar in Southern Algeria, Energy Procedia **42**, 53–62 (2013)
54. M.S. Adaramola, O.M. Oyewola, O.S. Ohunakin, O.O. Akinnawonu, Performance evaluation of wind turbines for energy generation in Niger Delta, Nigeria, Sustain. Energy Technol. Assess. **6**, 75–85 (2014)
55. E.K. Akpinar, S. Akpinar, An assessment on seasonal analysis of wind energy characteristics and wind turbine characteristics, Energy Convers. Manag. **46**, 1848–1867 (2005)
56. S.S. Paul, S.O. Oyedepo, M.S. Adaramola, Economic assessment of water pumping systems using wind energy conversions in the southern part of Nigeria, ENERGY Explor. Exploit. **30**, 1–18 (2012)
57. S. Rehman, T.O. Halawani, M. Mohandes, Wind power cost assessment at twenty locations in the kingdom of Saudi Arabia, Renew. Energy **28**, 573–583 (2003)
58. S. Mathew, Wind energy: fundamentals, resource analysis and economics, Berlin Heidelberg: Springer-Verlag, 2007
59. L.M. Ayompe, A. Duffy, An assessment of the energy generation potential of photovoltaic systems in Cameroon using satellite-derived solar radiation datasets, Sustain. Energy Technol. Assess. **7**, 257–264 (2013)
60. A. Ilinca, E. McCarthy, J.-L. Chaumel, J.-L. Rétiveau, Wind potential assessment of Quebec Province, Renew. Energy **28**, 1881–1897 (2003)

Cite this article as: Dieudonné Kaoga Kidmo, Bachirou Bogno, Kodji Deli, Michel Aillerie, Bello Pierre Ngoussandou, Economic assessment of WECS for water pumping systems in the North Region of Cameroon, Renew. Energy Environ. Sustain. **6**, 6 (2021)